Journal of Molecular Liquids 367 (2022) 120425

Contents lists available at ScienceDirect

Journal of Molecular Liquids

journal homepage: www.elsevier.com/locate/molliq

# Larger diameter selection of carbon nanotubes by two phase extraction using amphiphilic polymeric surfactant

Seokhyeon Son, Hyunjun Park, Woo-Dong Jang *, Sang-Yong Ju *

*Department of Chemistry, Yonsei University, 50 Yonsei-ro, Seodaemun-Gu, Seoul 03722, South Korea*

ARTICLE INFO

*Article history:*
Received 18 May 2022
Revised 10 July 2022
Accepted 18 September 2022
Available online 22 September 2022

*Keywords:*
Sorting
Single-walled carbon nanotube
Extraction
Polyoxazoline
Larger diameter selection

ABSTRACT

Aqueous two-phase extraction is instrumental for obtaining single-walled carbon nanotubes (SWNT) with uniform physical properties. This study reports that a nonionic amphiphilic poly(2-ethyloxazoline)-benzyl ether derivative (POBE-BzE) not only efficiently disperses SWNT in both water and *p*-xylene, but can also be utilized as a single-surfactant for partitioning SWNT in a water/*p*-xylene two-phase extraction in a diameter ($d_t$) selective manner. While individual POBE-BzE/SWNT dispersions exhibit similar photoluminescence positions from the SWNT, $d_t$-dependency occurs according to the solvent. Upon two-phase extraction, a $d_t$ SWNT >0.9 nm was mainly extracted to the *p*-xylene layer, and its partition coefficient was investigated by varying the phase transfer catalyst or sodium chloride amounts, where sodium chloride served as a better transfer agent. The $d_t$ selective behavior and its partition coefficient were rationalized by the tight and loose configurations of the BzE moiety in each medium. This novel amphiphilic polymeric surfactant and two-phase extraction may be useful for sorting SWNT and other nanomaterials according to their size.

© 2022 Elsevier B.V. All rights reserved.

## 1. Introduction

Aqueous two-phase extraction (ATPE) is instrumental for obtaining pure single-walled carbon nanotubes (SWNT) in terms of electronic type [1], chirality [2–4], and handedness [5,6]. The advantage of ATPE is its simple extraction process which does not require intricate equipment. In this scheme, the phase-separated poly(ethylene oxide) and dextran layers contain relatively hydrophilic and hydrophobic entities in each phase [7]. Modification of the hydrophilicity of SWNT using combinations of surfactants promotes the segregation of SWNT from one phase to another. The specificity of the surfactant binding affinity with SWNT chirality, termed (*n*, *m*) [8], and the subsequent change of hydrophilicity are responsible for the sorting of SWNT in the ATPE method [9,10]. However, the fine-tuning of hydrophilicity by using two surfactants inevitably changes the binding affinity and obscures the binding affinity difference with other SWNT chiralities. In this regard, one amphiphilic surfactant may be beneficial for sorting SWNT [11]. However, such amphiphilic surfactants must be carefully designed.

On the other hand, polyoxazoline formed by cationic ring-opening polymerization is a nonionic polymeric surfactant that is not significantly affected by an acid-base or large concentrations of electrolytes [12]. In particular, poly(2-ethyloxazoline) (POBE, Fig. 1A) is amphiphilic. Moreover, the modification of the side chain can tune the hydrophilicity [13–18]. Such phase behavior has been utilized to release nanoparticle structures [19]. Because of the excellent performance and tunability of nonionic polymeric surfactants, various block copolymer amphiphiles have been developed as polymeric surfactants [20–26].

In this contribution, we report that amphiphilic poly(2-ethyloxazoline)-benzyl ether derivative (POBE-BzE) not only efficiently disperses SWNT in both water and *p*-xylene, but can also be utilized as a single surfactant for partitioning POBE-BzE/SWNT from water to *p*-xylene in a diameter ($d_t$)-selective manner. The optical and morphological characteristics of the SWNT dispersions in water and *p*-xylene promoted by the polymer were investigated. Importantly, the $d_t$-selective extraction of the POBE-BzE /SWNT adduct from water to *p*-xylene was investigated by varying the phase-transfer catalyst or sodium chloride amount. A larger $d_t$ selectivity mechanism is proposed based on the interaction of the SWNT-interacting moiety with respect to the surrounding media.

* Corresponding authors.
*E-mail addresses:* wdjang@yonsei.ac.kr (W.-D. Jang), syju@yonsei.ac.kr (S.-Y. Ju).

https://doi.org/10.1016/j.molliq.2022.120425
0167-7322/© 2022 Elsevier B.V. All rights reserved.

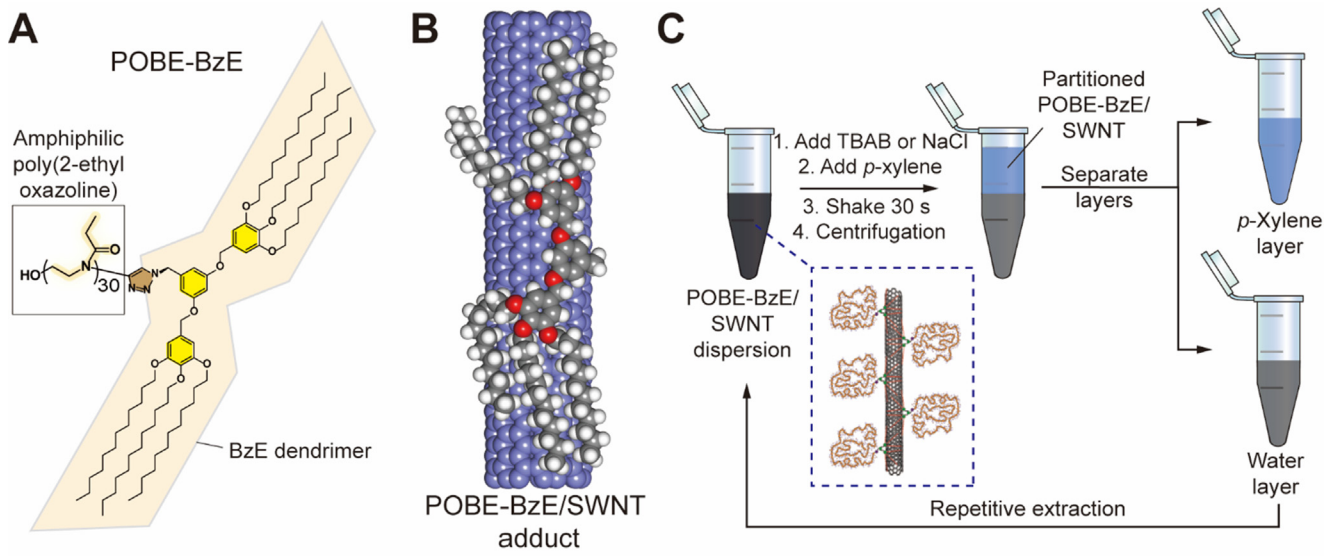


**Fig. 1.** POBE-BzE-assisted SWNT dispersion and its utilization for water/organic two-phase extraction. (A) Chemical structure of POBE-BzE. (B) Geometry-optimized adduct of a POBE-BzE on armchair (7,7) SWNT. Note that the POBE part is omitted. (C) Repetitive two-phase extraction procedure using water/*p*-xylene. For second extraction and more, neither TBAB nor NaCl were added to the water phase.

## 2. Experimental

### 2.1. Materials and equipment

poly(2-ethyl oxazoline)-alkylated 2nd generation benzyl ether (POBE-BzE) was prepared according to the literature [18], and exhibited a number-averaged molecular weight (Mn) of 4500 Da. TBAB was purchased from TCI (purity > 99 %, Japan). All reagents were of spectroscopic grade and used without further purification. Millipore quality deionized (DI) water with a resistivity > 18 MΩ was used for all the experiments. SWNT prepared using high-pressure carbon monoxide (HiPco) process [28] were purchased from NanoIntegris Inc. (Canada; raw grade, batch #: HR35-067, minimum SWNT content > 65 %) and had a median $d_t$ with distributions of 1.0 ± 0.3 nm. All the measurements were performed at 20 °C. $^1$H nuclear magnetic resonance (NMR) spectra were recorded using a Bruker DPX 300 (300 MHz) or Bruker DPX 400 (400 MHz) spectrometer in $CDCl_3$. Analytical size exclusion chromatography (*SEC*) was performed using a JASCO HPLC equipped with HF-403HQ and HF-404HQ columns (Shodex, Japan) using tetrahydrofuran as the eluent. Matrix-assisted laser desorption ionization-time-of-flight mass spectroscopy (MALDI-TOF MS) was performed using a Bruker model LRF20 with 1,8,9-trihydroxyanthracene (dithranol) or *trans*-2-[3-(4-tert-butylphenyl)-2-methyl-2-propenylidene]malononitrile as the matrix and lithium trifluoroacetate or potassium iodide as the salt. Molecular simulation and geometry optimization were performed using the Gaussian 09 package with DFT/B3LYP with the 6-31G+(d,p) basis set.

### 2.2. Preparation of POBE-BzE/SWNT dispersions

POBE-BzE (67 mg) was added to DI water (10 mL) and agitated using a vortex mixer (Vortex Genie 2; Fisher Scientific, USA) until complete dissolution. HiPco SWNT (1 mg) was added to the mixed solution containing POBE-BzE. The resulting mixture was subjected to an approximately 30 min bath sonication (Branson 1510, 70 W, Emerson, USA) for initial mixing, followed by tip sonication for 1 h (40 % power, 30 W/mL (or 300 W per 10 mL), probe tip diameter of 13 mm, VCX 750; Sonics & Materials, USA) equipped with an external air cooler for the sonicator head. During sonication, the temperature of the sample vials was maintained at 20 °C using an external water circulator (RW-2025G, Lab Companion, Republic of Korea). Large bundles of HiPco SWNT, along with metal impurities, were discarded by a 5000 *g* centrifugation with a bench-top centrifuge (WiseSpin CF-10, Witeg Labortechnik GmbH, Germany; maximum force: 12,225 *g*) using 1.5 mL Eppendorf tubes at 20 °C. The resulting dispersion was black, and 80 % of the supernatant was carefully collected for measurement. Similarly, an ethylene glycol dispersion was prepared. For the *p*-xylene dispersion (10 mL), a larger amount of POBE-BzE (335 mg) and a lower centrifugal force (1000 *g*) were utilized to form a stable dispersion. *Attempted SWNT dispersion using POBE only*: We conducted a control experiment using only POBE with same molecular weight. HiPco SWNT (1 mg) was added to the mixed solution (10 mL) containing POBE without BzE (67 mg) in similar protocol mentioned above (bath sonication 30 min, tip sonication 1 h, centrifugation at 5000 *g* for 1 h).

### 2.3. Absorption measurement

The absorption spectra were acquired on a double-beam spectrophotometer (V-770, JASCO, Japan) using cuvettes with a 1 mm path length (21/Q/1, Starna Scientific, UK), unless otherwise noted. Absorption bleaching experiments were performed by adding a diluted HCl solution into the as-prepared POBE-BzE/SWNT/water dispersions to prepare have pH of 6.8, 5.1 and 3.0.

### 2.4. Photoluminescence excitation (PLE) measurement

PLE measurements were conducted using a Spex Nanolog 3–211 spectrofluorometer (Jobin Yvon, Horiba, Japan) according to the literature [10,27,28]. A 450 W xenon lamp was used as a light source. Emissions from a sample were collected using an LN-cooled InGaAs array detector (512 × 1 pixels, SymphonyII IGA, Horiba, Japan) in the NIR range. Wavelength calibration was conducted using a 467 nm peak originating from a xenon lamp. Both the excitation and emission light intensities were corrected against instrumental variations using sensitivity correction factors. For the measurement of the SWNT PL, the bandwidths of the excitation and emission wavelengths were 14 and 10 nm, respectively. The

excitation and emission wavelengths increased by 1 or 5 nm for 550–800 nm, and 1 nm for 900–1350 nm, respectively. A fluorescence quartz cuvette (QS, Hellma) with a 10 mm beam pass length was utilized for the measurements. All measurements were conducted at 20 °C. The PL intensity of the recorded spectra was adjusted by a dilution factor and accumulation time. The Origin program implemented in FluorEssence™ was used to analyze the PL spectra. A fluorescence cuvette with 50 μL (16.50-F/Q/10, Starna Scientific, UK) was used.

### 2.5. Two-phase extraction

All two-phase extractions were conducted in 1.5 mL Eppendorf tubes (Microtubes, MCT-150-C, Axygen, USA). Aqueous POBE-BzE/SWNT dispersions (0.5 mL) were thoroughly mixed with varying amounts of TBAB (0, 1.9, 2.5, 3.1, 3.7, 4.3, 5.0, 5.6 and 6.2 mM) as a phase-transfer catalyst to transfer POBE-BzE/SWNT to another phase. 6.2 mM TBAB showed the best partition constant. Pure *p*-xylene (0.5 mL) was added to the tube. The tube was thoroughly mixed using a vortex mixer (1 min) and allowed to settle for 10 min. A further settle-down process was applied using a low centrifugal force (1000 *g*) for 5 min. The lower aqueous and upper organic phases were carefully collected for other measurements. For repetitive extraction, the bottom water layer from the previous step was utilized to extract further with the organic layer. Similarly, varying amounts of NaCl (that is, 3.1, 3.7, 4.3, 4.9, 5.5, and 6.1 mM) were added for two-phase extraction. 4.3 mM NaCl displays continuous extraction without SWNT aggregation.

### 2.6. Atomic force microscopy (AFM) measurement

AFM measurements were conducted using a commercially available AFM (NX10, Park systems, Republic of Korea). An Al-coated Si cantilever with a spring constant of 37 N/m, resonance frequency of 300 kHz, and quoted radius of approximately 6 nm (ACTA, App Nano, USA) was utilized to measure the height topographies. Typically, a 512 × 512 pixel image was collected from a 3 μm × 3 μm area. Prior to the AFM measurements, the POBE-BzE/SWNT water and *p*-xylene dispersions were deposited on a 285 nm-thick $SiO_2$/Si substrate by dipping for 10 min. Each substrate was then rinsed with the respective solvent (that is, water and *p*-xylene) several times and dried under a $N_2$ stream. The measured height and phase topographies were analyzed using the XEI 4.3.4 program (Park systems, Republic of Korea). *Determination of length distribution*: We only consider individual POBE-BzE/SWNT based on the 3-nm height considering average SWNT diameter (~1 nm), thickness of POBE-BzE (0.34 nm × 2), van der Waals distance (0.34 nm × 2) of individualized POBE-BzE/SWNTs. About 20 AFM images contains >100 individualized POBE-BzE/SWNT were analyzed and averaged via freeware ImageJ program.

## 3. Results

Fig. 1A and 1B illustrates the chemical structures of POBE-BzE and POBE-BzE assembly on the SWNT, respectively. The chemical structure of POBE-BzE (Fig. 1A) consists of POBE and an alkylated benzyl ether (that is, 1,3-bis((3,4,5-tris(dodecyloxy)benzyl)oxy)benzene)) linked by a triazole through a Click reaction. This polymer was synthesized according to the literature [18]. The synthesized POBE-BzE was characterized by $^1$H NMR spectroscopy, MALDI-TOF MS and *SEC*. The $^1$H NMR spectrum indicated the formation of a triazole linkage between POBE and BzE, as evidenced by the triazole CH peak and chemical shifts of the methylene peaks near the triazole linkage, indicated by the blue and yellow solid circles (Fig. S1). The MS spectrum (Fig. S2) shows a series of peaks at regular intervals of 99 Da, which is the molecular weight of monomeric 2-ethyl oxazoline. Additionally, the number-averaged molecular weight and dispersity index ($Đ$) were estimated as 4500 Da and 1.08, respectively. The *SEC* retention time profile also exhibited a narrow molecular weight distribution (Fig. S3). In particular, alkylated benzyl ether has a badge shape that allows wrapping of the SWNT surface by hydrophobic interactions, as shown in Fig. 1B. The POBE moiety is amphiphilic, and its solvents include water, anisole, benzene, chloroform, cyclohexane, dichloromethane, ethyl acetate, hexane, *p*-xylene, and toluene. Among those solvents, water and *p*-xylene were elected since they are immiscible with water and have the lowest solubility in each other, as shown in Fig. S4 [29]. Upon non-covalent functionalization of POBE-BzE with SWNT, the BzE moiety wraps around the SWNT, as shown in the geometry-optimized structure in Fig. 1B.

HiPco SWNT, whose $d_t$ is 1.0 ± 0.3 nm [30], were dispersed in the following manner: a mixture of HiPco (1 mg), POBE-BzE (67 mg), and DI water (10 mL) was subjected to an initial 30 min bath sonication for homogenization, and then probe sonication for 1 h at 300 W for dispersion. Then, 5000 gravitational acceleration (*g*) centrifugation was conducted to discard the larger SWNT bundles and metal catalyst, and 80 % of the supernatant was collected. Similarly, POBE-BzE with a higher concentration (that is, 335 mg) was used to disperse SWNT in *p*-xylene, although a significantly lower centrifugal force (1000 *g*) was required to obtain the dispersion. Fig. 2A shows the UV–vis-near IR (NIR) absorption spectra of the POBE-BzE/SWNT dispersions in water (black curve) and *p*-xylene (red curve). The benzyl ether moiety of POBE has a strong absorption below 300 nm and allows clean visible and NIR ranges without overlapping with the optical transitions of the SWNT. Additionally, profound bands originating from individual SWNTs were found in the rest of the spectra. The first and second excitonic transitions of the semiconducting SWNT ($e^S_{11}$ and $e^S_{22}$) are situated in the 950–1350 and 600–950 nm regions, respectively, whereas the first excitonic transitions of the metallic SWNT ($e^M_{11}$) are situated in the 450–600 nm region. These results are in accordance with the literature [31]. The water dispersion exhibited the strongest $e^S_{11}$ absorption at approximately 1150 nm, whereas that of the *p*-xylene dispersion occurred at approximately 1300 nm. This result is the first indication that water and *p*-xylene dispersions have different SWNT selections for SWNT chirality.

PLE maps clearly indicated the solvent-induced $d_t$ selectivity. Fig. 2B and 2C show the resulting PLE maps of the POBE-BzE/SWNT dispersion in water and *p*-xylene. PLE maps were utilized to determine the $e^S_{11}$ and $e^S_{22}$ of each semiconducting SWNT chirality [28], denoted as ($n$, $m$), from the POBE-BzE/SWNT dispersions in different media. Table S1 lists the $e^S_{11}$ and $e^S_{22}$ from each dispersion. A comparison of the PLE maps shows that the *p*-xylene layer has a larger $d_t$ selectivity. For instance, while the water dispersion exhibits the maximum photoluminescence (PL) intensity ($I_{PL}$) from the (8,4) chirality (that is, $d_{t,\,(8,4)}$ = 0.84 nm), the *p*-xylene dispersion exhibits the maximum $I_{PL}$ from the (9,5), (10,3), and (11,1) chiralities (that is, $d_{t,\,(9,5)}$ = 0.98 nm, $d_{t,\,(10,3)}$ = 0.94 nm, and $d_{t,\,(11,1)}$ = 0.92 nm). Moreover, the (9,5), (10,3) and (11,1) species in *p*-xylene exhibited an $e^S_{11}$ at 1280, 1288 and 1298 nm, respectively. PL-intensity based chirality abundances of SWNT in each medium (Fig. S5A and S5B) were plotted as Weisman plots in Fig. 2D and 2E. Clearly, *p*-xylene dispersion as compared to water dispersion exhibits larger $d_t$ enrichment whose most abundant species are (9,5) as 15.2 %. These results are consistent with the larger $d_t$ enrichment observed in the absorption results. Moreover, POBE-BzE/SWNT in water exhibited a blue-shifted trend with an average of 4 meV for $e^S_{11}$, as compared to those in *p*-xylene (Table S1 and Fig. 2F). This change is within the range of SWNT solvatochromism [27,32,33]. Moreover, a control experiment was conducted to determine whether the POBE homopolymer is

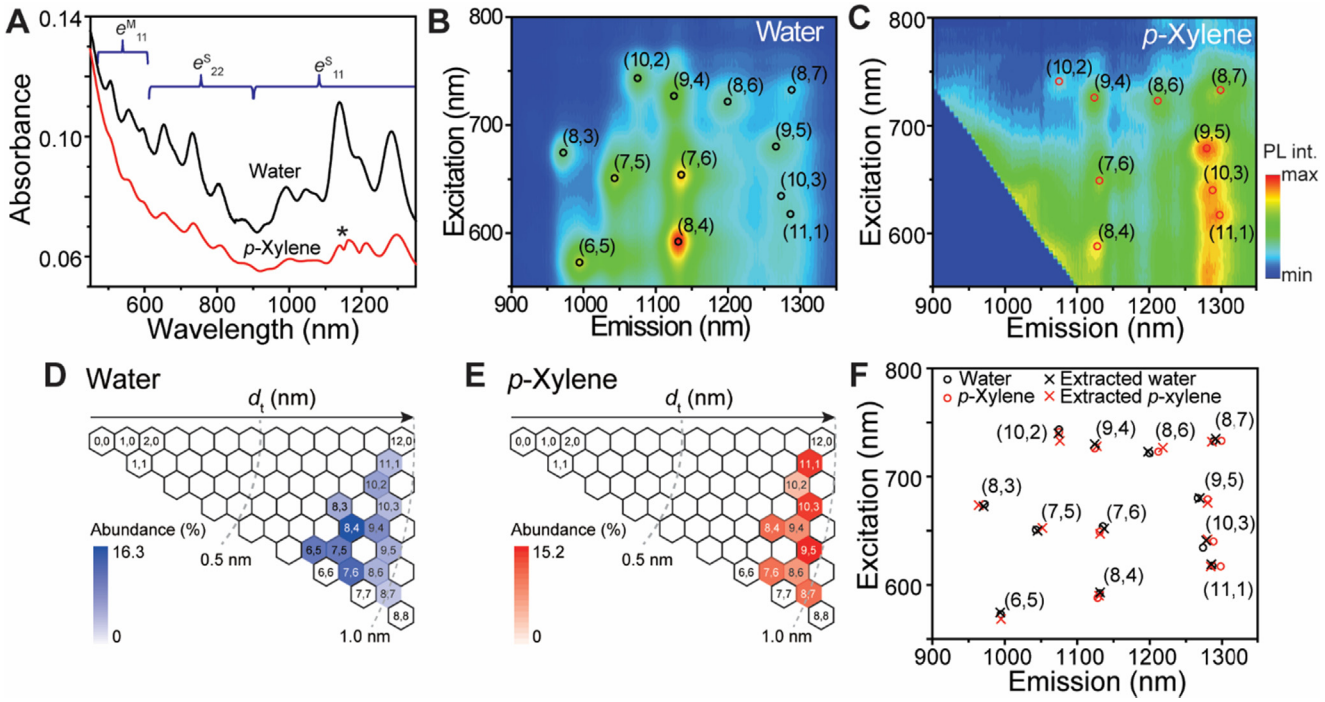


**Fig. 2.** Spectroscopic characterizations of POBE-BzE/SWNT dispersions in water and *p*-xylene. (A) UV–vis-NIR absorption spectra of POBE-BzE/SWNT dispersions in water (black) and *p*-xylene (red). The asterisk denotes absorption from residual water. PLE maps of POBE-BzE/SWNT dispersions in (B) water and (C) *p*-xylene. Crosspoint of $e^{S}_{11}$ and $e^{S}_{22}$ of each SWNT (*n*, *m*) are denoted as circles. (D and E) Weisman plots of PL-based (*n*, *m*) chirality abundance of SWNT in each medium. (F) The $e^{S}_{11}$ and $e^{S}_{22}$ trends of the POBE-BzE/SWNT dispersion in water (black circles), *p*-xylene (red circles), water extraction (black crosses), and *p*-xylene extraction (red crosses).

responsible for SWNT dispersion. The POBE-BzE/SWNT dispersion in water and *p*-xylene prepared using a similar preparation protocol did not yield a dispersion, as evident by photograph, absorption and PLE maps (Fig. S6A, S6B, and S6C to S6D, respectively). This suggests that the BzE moiety is responsible for the SWNT interactions, as depicted in Fig. 1A. Even more, to check the possibility for absorption bleaching of POBE-BzE/SWNT/water, pH-dependent absorption measurements were performed.[34] Interestingly, pH change from the as-prepared 6.8, 5.1 and 3.0 does not show any $d_t$-dependent bleaching of $e^{S}_{11}$ in both absorption and PLE maps (Fig. S7A to S7D), suggesting no bleaching occurring.

Next, the morphology of the POBE-BzE/SWNT adduct was investigated using AFM. Fig. 3A shows the height topography of the POBE-BzE/SWNT/water dispersion deposited on a 285 nm-thick $SiO_2$/Si substrate. The topography clearly indicates that the SWNT was wrapped by a random assembly of POBE-BzE. The heights (Fig. 3B) of the individual and lightly bundled SWNT were 2 and 5 nm, respectively. Considering the $d_t$ distribution of HiPco, such a line profile indicates individualized SWNT with POBE-BzE wrapping as small as 0.7 nm, which is twice the van der Waals distance between the SWNT and polymer wrapping. Furthermore, the length distribution obtained by analyzing 102 tubes (Fig. 3C) was well-fitted with a lognormal distribution and displayed an average length of 0.18 μm. In contrast, the topography of the POBE-BzE/SWNT/*p*-xylene dispersion (Fig. 3D) exhibited a significantly lower height spanning from 1 to 3 nm (Fig. 3E), suggesting a thin POBE-BzE wrapping. This result suggests that the POBE-BzE wrapping does not fully cover the sidewalls of the SWNT. The measured average length was 0.16 μm, which is similar to that derived from the water dispersion. This result indicates that POBE-BzE has different affinities for SWNT in water and *p*-xylene.

The amphiphilicity of POBE-BzE/SWNT prompted the demonstration of a two-phase (that is, water/*p*-xylene) extraction. Efficient extraction of POBE-BzE/SWNT with *p*-xylene was promoted by the addition of 6.2 mM tetrabutylammonium bromide (TBAB), a phase transfer catalyst, at the water/aromatic solvent interface. Extraction without TBAB resulted in nearly no POBE-BzE/SWNT being transferred into the *p*-xylene layer and increasing the TBAB concentration (from 1.9 to 6.2 mM) resulted in increased SWNT concentration, as shown in the absorption spectra in Fig. S8. Fig. 4A shows a photograph of a series of Eppendorf tubes with extraction numbers from 1 to 10. As the number of extractions increased, the water layer displayed progressively reduced optical density and concentrations of POBE-BzE/SWNT. Fig. 4B and 4C display the offset absorption spectra of the water and *p*-xylene layers, respectively. With an increase in the number of extractions, the absorption of the water layer decreased, whereas that of the *p*-xylene layer increased. This result clearly indicates that TBAB promotes the transfer of POBE-BzE/SWNT from water to *p*-xylene.

The extraction of POBE-BzE/SWNT from water to the *p*-xylene layer can be explained by the partition coefficient ($K$) which is given as follows [7]: $K = c_{top}/c_{bottom}$, where $c_{top}$ and $c_{bottom}$ represent the concentrations of SWNT in the top and bottom layers, respectively. For this, the peaks of each absorption were subtracted from the background absorption (see Fig. S9). Table 1 lists the $K$ values of each peak, along with the $K$ values from the 4.3 mM NaCl addition, which will be discussed later. In the 6.2 mM TBAB system, $K$ of $e^{M}_{11}$ and $e^{S}_{22}$ slightly increased for peaks with longer wavelengths, suggesting that the sorting based on two-phase extraction has a $d_t$ dependency.

Although POBE-BzE with TBAB promoted the extraction of SWNT in the *p*-xylene layer, the $K$ value of each peak was at the $10^{-3}$ level. Further promotion of the transfer to *p*-xylene was achieved by adding NaCl to the aqueous phase. NaCl is known to promote the salting-out effect in aqueous media [35]. For this, 3.1–6.1 mM NaCl was added to each vial. Fig. 5A shows a photograph of the vials after extraction. The *p*-xylene phase has a considerably darker optical density and, upon increasing the NaCl concentration, further promotes POBE-BzE/SWNT transfer. It was noticed that NaCl concentrations of 4.9 mM and above induced

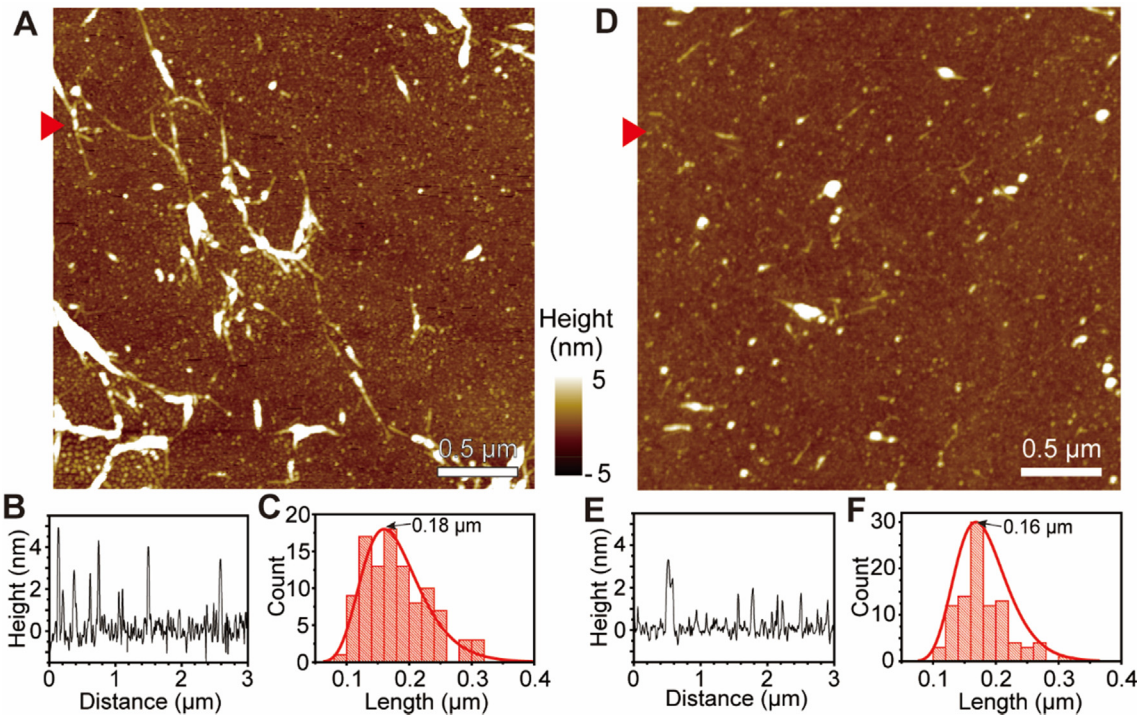


**Fig. 3.** Topographies of POBE-BzE/SWNT water and *p*-xylene dispersions deposited on a 285 nm-thick $SiO_2$/Si substrate. The samples were washed with the respective solvents several times. (A) Height topography of the water dispersion, and (B) line profile and (C) length histogram from the water dispersion. (D–F) Similar measurements for the *p*-xylene dispersion.

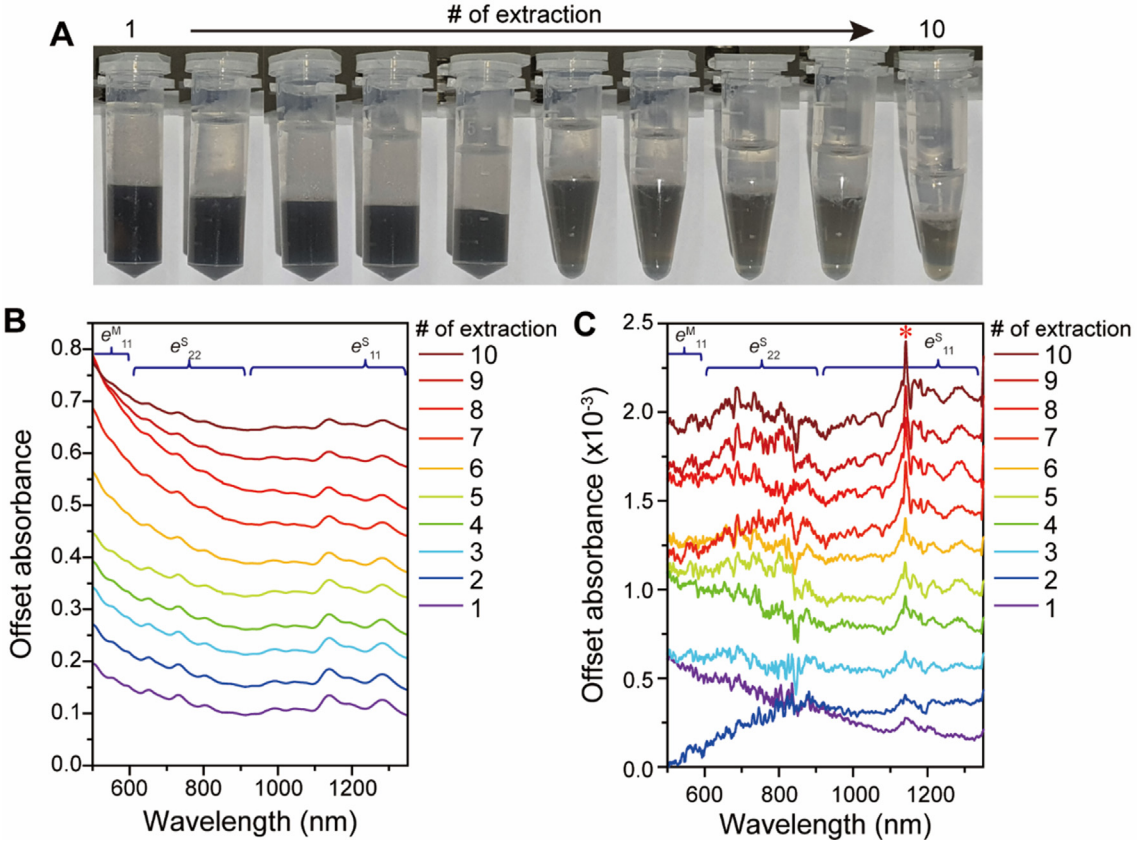


**Fig. 4.** Repetitive extractions of POBE-BzE/SWNT/water dispersion to *p*-xylene in the presence of 6.2 mM TBAB. (A) Photograph of a series of repetitive two-phase extractions. (B) Absorption spectra of the extracted water layer. Each spectrum is offset by 0.05 for visual clarity. (C) Absorption spectra of the extracted *p*-xylene layer. Each spectrum is offset by $0.2 \times 10^{-3}$ for visual clarity. The asterisk indicates residual water contained in *p*-xylene during extraction.

**Table 1**
*K* determined by the peak ratio in the water and *p*-xylene layer absorption spectra according to $e_{11}^{M}$, $e_{22}^{S}$, and $e_{11}^{S}$ of 6.2 mM TBAB- and 4.3 mM NaCl-assisted repetitive extractions. The asterisks indicate uncertainty.

| System | | | $e_{11}^{M}$ (nm) | | $e_{22}^{S}$ (nm) | | | | $e_{11}^{S}$ (nm) | | | |
|---|---|---|---|---|---|---|---|---|---|---|---|---|
| | | | ~554 | ~596 | ~652 | ~731 | ~804 | ~877 | ~992 | ~1045 | ~1139 | ~1282 |
| 6.2 mM TBAB | Peak abs. ($\times10^{-5}$) | Water | 227 | 145 | 525 | 673 | 368 | 179 | 367 | 133 | 1547 | 1374 |
| | | *p*-Xylene | 7 ± 3.2 | 4 ± 3.7 | 9 ± 4.7 | 10 ± 2.6 | 12 ± 8.1 | 10 ± 5.6 | 4 ± 1.8 | 4 ± 1.6 | 16 ± 3.3 | 6 ± 1.3 |
| | *K* ($\times10^{-3}$) | | 21 ± 10 | 22 ± 18 | 12 ± 6 | 10 ± 3 | 23 ± 16 | 52 ± 30 | 7 ± 3 | 14 ± 6 | 7 ± 1 | 3 ± 0.7 |
| 4.3 mM NaCl | Peak abs. ($\times10^{-3}$) | Water | 96 | 69 | 125 | 181 | 149 | 81 | 37 | 39 | 292 | 364 |
| | | *p*-Xylene | 9 | 7 | 12 | 20 | 17 | 9 | 4 | 4 | 24 | 42 |
| | *K* ($\times10^{-2}$) | | 9.8 | 9.9 | 9.6 | 10.8 | 11.3 | 10.7 | 10.1 | 9.1 | 8.3 | 11.6 |

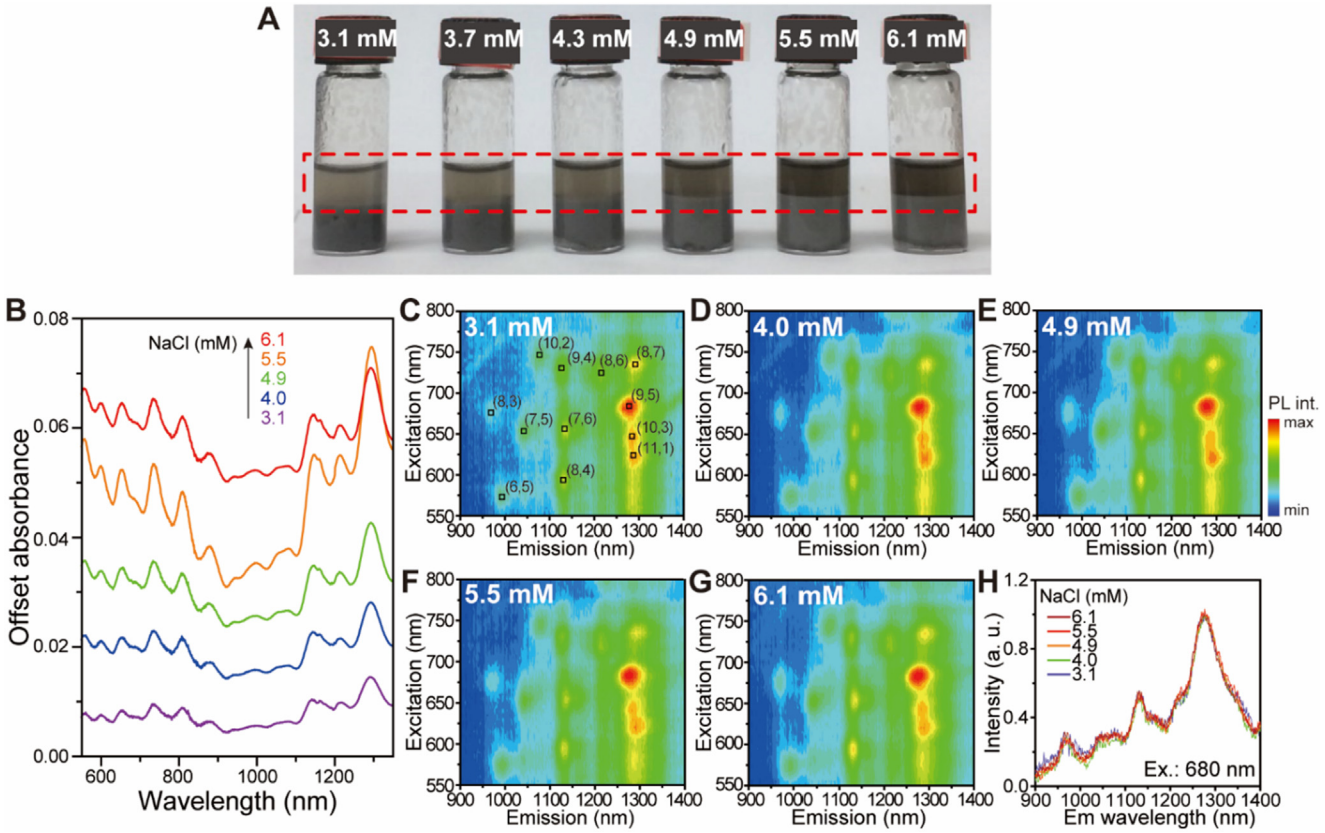


**Fig. 5.** NaCl-assisted two phase extraction of POBE-BzE/SWNT from water to *p*-xylene with increasing NaCl concentrations. (A) Photograph of layered water/*p*-xylene samples according to increasing NaCl concentrations. The red box denotes the *p*-xylene layer. (B) The offset absorption spectra of the extracted *p*-xylene layer. Each spectrum is offset by 0.05 for visual clarity. (C-G) PLE maps of the extracted *p*-xylene layer. (H) PL emission spectra excited at 680 nm.

SWNT aggregation in the bottom phase. Therefore, 4.3 mM NaCl was selected for the remainder of the study. The extracted *p*-xylene layer showed a large SWNT absorption, as shown in Fig. 5B. The offset absorption spectra display that 5.5 mM NaCl induces maximum SWNT transfer. The large absorption at 1300 nm indicates the enrichment of larger $d_t$ SWNT. The corresponding PLE maps show that enrichment of individualized large $d_t$ SWNT occurs. Fig. 5C-5G display PLE maps of the *p*-xylene layers. All PLE maps display the enrichment of large $d_t$ SWNTs centered on the aforementioned tube with an average $d_t$ = 0.95 nm for the (8,7), (9,5), (10,2), and (11,3) species. Similar results were observed in the PL emission spectra (Fig. 5H), in which the spectra displayed similar chirality distributions regardless of the extraction number. This result indicates that efficient extraction was promoted by the addition of NaCl.

A series of two-phase extractions were performed in the presence of 4.3 mM NaCl. Fig. 6A shows a photograph of the extracted *p*-xylene layer. Based on the optical density, up to three rounds of extraction enabled the efficient extraction of SWNT in water. Moreover, the resulting absorption spectra (Fig. 6B) showed that three consecutive extractions were sufficient for the extraction. The absorption at 1300 nm was the highest among the $e_{11}^{S}$ peaks. The resulting PLE maps (Fig. 6C–6G) and the PL emission spectra excited at 680 nm (Fig. 6H) show that all the PLE maps display a larger $d_t$ enrichment of SWNT regardless of the number of extractions, indicating that extraction with *p*-xylene is fairly $d_t$ selective.

## 4. Discussion

The aforementioned larger $d_t$ SWNT selectivity of POBE-BzE in *p*-xylene attributes this selection to the interaction of POBE-BzE with the surrounding media. Fig. 1A shows that BzE has six *n*-dodecyl chains and three benzene rings. In the water dispersion, water pushes the BzE moiety to the SWNT surface. Therefore, POBE-BzE selects a smaller $d_t$ SWNT. In contrast, *p*-xylene, which is a good solvent with *n*-dodecyl moiety of BzE, [27] attracts the

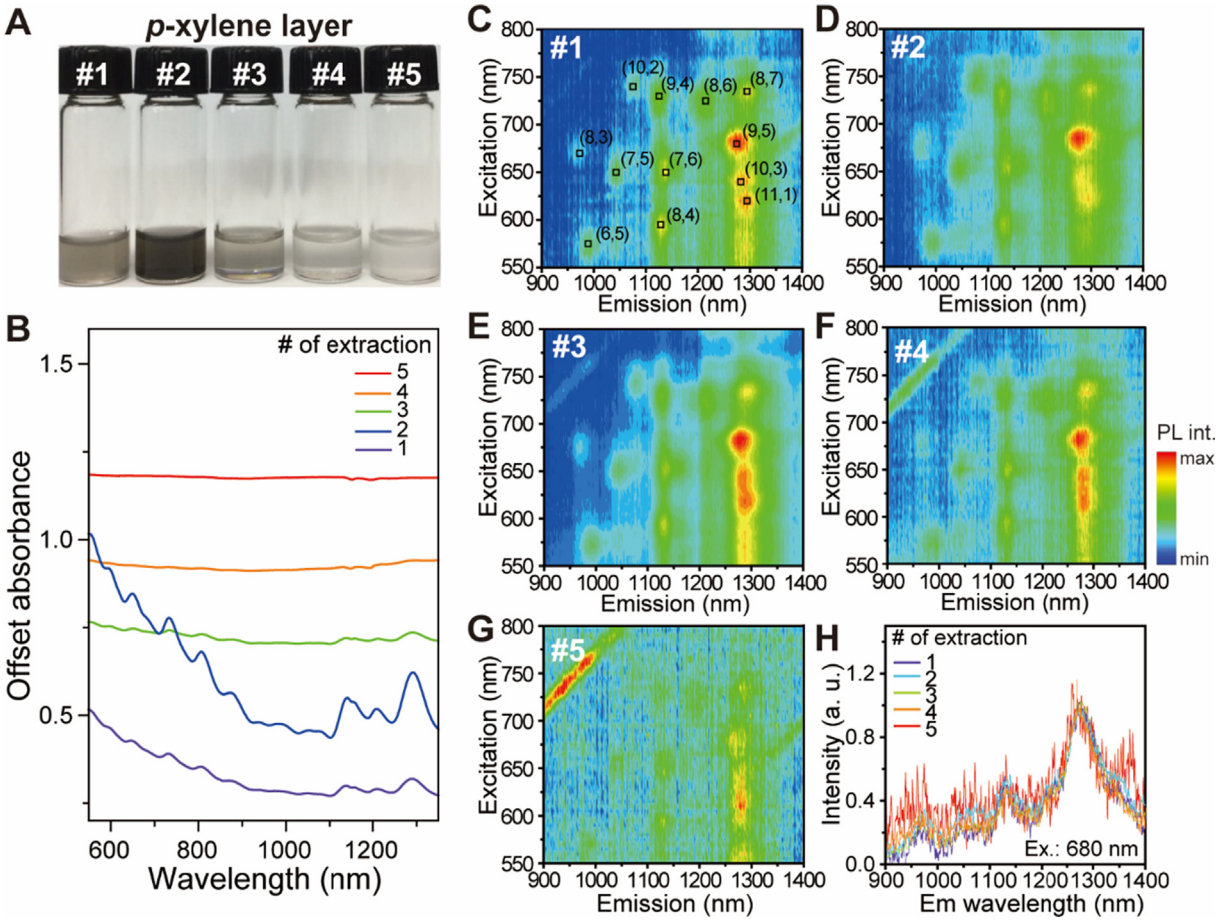


**Fig. 6.** Repetitive two-phase extractions from water to *p*-xylene in the presence of 4.3 mM NaCl. (A) Photograph of the *p*-xylene layers with an increasing number of extractions. (B) Absorption spectra of the extracted *p*-xylene. Each spectrum is offset by 0.2 for visual clarity. (C-G) PLE maps of the extracted *p*-xylene layer. (H) PL emission spectra of the extracted *p*-xylene layers after several extractions.

BzE moiety to the media, resulting in a loosely packed BzE configuration. These results support the fact that a higher POBE-BzE concentration is necessary for SWNT dispersion in *p*-xylene only. Therefore, the relatively loosely bound BzE moiety can accommodate SWNT with larger $d_t$. Moreover, when free POBE-BzE was added to *p*-xylene, the resulting water extract does not show proportional increase in POBE-BzE absorbance at 276 nm (Fig. S10). This result indicates that preferential partition of POBE-BzE towards *p*-xylene is partial reason for extraction from water to *p*-xylene. This additional aspect explains why the observed *K* shows an increasing value for SWNT with larger $d_t$, as shown in Fig. 7. These results correspond with the aforementioned selectivity for SWNTs with larger $d_t$.

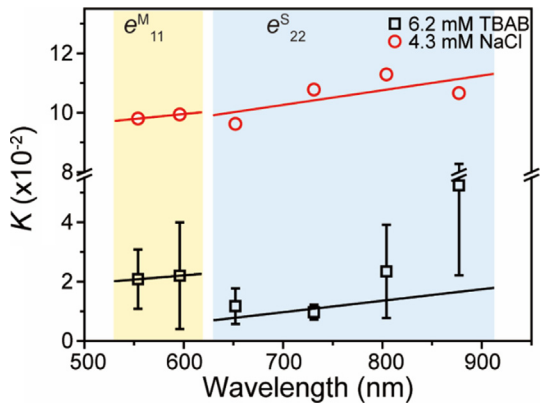


**Fig. 7.** Trend of *K* of (A) 6.2 mM TBAB- and (B) 4.3 mM NaCl-assisted extractions. Each curve was linear fitted according to the optical transitions.

## 5. Conclusion

It was found that POBE-BzE is an efficient nonionic amphiphilic surfactant of SWNT in aqueous *p*-xylene and extracted from water to *p*-xylene. The absorption and PL spectra show that POBE-BzE/SWNT in both solvents exhibit similar optical transitions, albeit with different $d_t$ selectivities. The AFM results show that POBE-BzE in water is more robust on SWNT than in organic dispersions. The presence of TBAB or NaCl promoted the transfer of POBE-BzE/SWNT from water to *p*-xylene and increased the partition coefficient up to 0.1. Moreover, the extraction of *p*-xylene was more $d_t$-selective. The solvent-specific $d_t$ selectivity was attributed to the tight and loose configurations of the BzE unit in water and *p*-xylene media. This two-phase extraction will be useful for sorting not only SWNT, but also other nanomaterials.

## Data availability

Data will be made available on request.

## Declaration of Competing Interest

The authors declare that they have no known competing financial interests or personal relationships that could have appeared to influence the work reported in this paper.

## Acknowledgments

This research was financially supported by the Basic Science Research Program through the National Research Foundation of Korea (NRF), funded by the Ministry of Education, Science, and Technology (NRF-2022R1A2C1006932 and NRF-2020R1A4A101773711).

## Appendix A. Supplementary data

**Supporting Information available:** $^1$H NMR spectrum of POBE-BzE (Fig. S1), MALDI-TOF mass spectrum of POBE-BzE (Fig. S2), elution profile of POBE-BzE by SEC (Fig. S3), solubility of various solvents in water (Fig. S4), PL-based chirality abundances from water and *p*-xylene phases (Fig. S5), Attempt to disperse HiPco SWNT by using POBE (Fig. S6), pH-dependent absorption and PL changes of POBE-BzE/SWNT/water dispersion (Fig. S7), offset absorption spectra after extraction with varying amounts of TBAB (Fig. S8), determination of the peak (red line) from the background absorption (Fig. S9), preference of POBE-BzE in *p*-xylene (Fig. S10) and deconvoluted $e_{11}^S$ and $e_{22}^S$ of the SWNT chiralities in each dispersion (Table S1) are available. Supplementary data to this article can be found online at https://doi.org/10.1016/j.molliq.2022.120425.

## References

[1] C.Y. Khripin, J.A. Fagan, M. Zheng, Spontaneous partition of carbon nanotubes in polymer-modified aqueous phases, J. Am. Chem. Soc. 135 (18) (2013) 6822–6825.
[2] J.A. Fagan, C.Y. Khripin, C.A. Silvera Batista, J.R. Simpson, E.H. Hároz, A.R. Hight Walker, M. Zheng, Isolation of specific small-diameter single-wall carbon nanotube species via aqueous two-phase extraction, Adv. Mater. 26 (18) (2014) 2800–2804.
[3] G. Ao, C.Y. Khripin, M. Zheng, DNA-controlled partition of carbon nanotubes in polymer aqueous two-phase systems, J. Am. Chem. Soc. 136 (29) (2014) 10383–10392.
[4] J.A. Fagan, E.H. Hároz, R. Ihly, H. Gui, J.L. Blackburn, J.R. Simpson, S. Lam, A.R. Hight Walker, S.K. Doorn, M. Zheng, Isolation of >1 nm diameter single-wall carbon nanotube species using aqueous two-phase extraction, ACS Nano 9 (5) (2015) 5377–5390.
[5] G. Ao, J.K. Streit, J.A. Fagan, M. Zheng, Differentiating left- and right-handed carbon nanotubes by DNA, J. Am. Chem. Soc. 138 (51) (2016) 16677–16685.
[6] H. Li, G. Gordeev, O. Garrity, N.A. Peyyety, P.B. Selvasundaram, S. Dehm, R. Krupke, S. Cambré, W. Wenseleers, S. Reich, M. Zheng, J.A. Fagan, B.S. Flavel, Separation of specific single-enantiomer single-wall carbon nanotubes in the large-diameter regime, ACS Nano 14 (1) (2020) 948–963.
[7] P.-Å. Albertsson, Partition of Cell Particles and Macromolecules in Polymer Two-Phase Systems, in: C.B. Anfinsen, J.T. Edsall, F.M. Richards (Eds.), Adv. Protein Chem., Academic Press: 1970; Vol. 24, pp 309-341.
[8] N. Hamada, S.-I. Sawada, A. Oshiyama, New one-dimensional conductors: graphitic microtubules, Phys. Rev. Lett. 68 (10) (1992) 1579–1581.
[9] S.-Y. Ju, J. Doll, I. Sharma, F. Papadimitrakopoulos, Selection of carbon nanotubes with specific chiralities using helical assemblies of flavin mononucleotide, Nat. Nanotechnol. 3 (6) (2008) 356–362.
[10] M. Park, J. Park, J. Lee, S.-Y. Ju, Scaling of binding affinities and cooperativities of surfactants on carbon nanotubes, Carbon 139 (2018) 427–436.
[11] H. Oh, J. Sim, S.-Y. Ju, Binding affinities and thermodynamics of noncovalent functionalization of carbon nanotubes with surfactants, Langmuir 29 (35) (2013) 11154–11162.
[12] S. Penczek, G. Moad, Glossary of terms related to kinetics, thermodynamics, and mechanisms of polymerization (IUPAC recommendations 2008), Pure Appl. Chem. 80 (10) (2008) 2163–2193.
[13] Y. Jung, W.-D. Jang, Recent approaches for clickable poly(2-oxazoline)-based functional stimuli-responsive polymers and related applications, Supramol. Chem. 29 (10) (2017) 714–722.
[14] T. Lorson, M.M. Lübtow, E. Wegener, M.S. Haider, S. Borova, D. Nahm, R. Jordan, M. Sokolski-Papkov, A.V. Kabanov, R. Luxenhofer, Poly(2-oxazoline)s based biomaterials: a comprehensive and critical update, Biomaterials 178 (2018) 204–280.
[15] M.A. Mees, R. Hoogenboom, Full and partial hydrolysis of poly(2-oxazoline)s and the subsequent post-polymerization modification of the resulting polyethylenimine (co)polymers, Polym. Chem. 9 (40) (2018) 4968–4978.
[16] T.R. Dargaville, J.-R. Park, R. Hoogenboom, Poly(2-oxazoline) hydrogels: state-of-the-art and emerging applications, Macromol. Biosci. 18 (6) (2018) 1800070.
[17] A. Bordat, T. Boissenot, J. Nicolas, N. Tsapis, Thermoresponsive polymer nanocarriers for biomedical applications, Adv. Drug Deliv. Rev. 138 (2019) 167–192.
[18] J.H. Joe, J.M. Park, H. Lee, W.-D. Jang, A dendritic-linear block copolymer as a thermoresponsive non-ionic polymer surfactant, Eur. Polym. J. 118 (2019) 320–326.
[19] P. Wilson, P.C. Ke, T.P. Davis, K. Kempe, Poly(2-oxazoline)-based micro- and nanoparticles: a review, Eur. Polym. J. 88 (2017) 486–515.
[20] K.A. Davis, K. Matyjaszewski, Atom transfer radical polymerization of tert-butyl acrylate and preparation of block copolymers, Macromolecules 33 (11) (2000) 4039–4047.
[21] Q. Ma, K.L. Wooley, The preparation of t-butyl acrylate, methyl acrylate, and styrene block copolymers by atom transfer radical polymerization: precursors to amphiphilic and hydrophilic block copolymers and conversion to complex nanostructured materials, J. Polym. Sci. A 38 (S1) (2000) 4805–4820.
[22] O. Colombani, M. Ruppel, F. Schubert, H. Zettl, D.V. Pergushov, A.H. Müller, Synthesis of poly (n-butyl acrylate)-block-poly (acrylic acid) diblock copolymers by ATRP and their micellization in water, Macromolecules 40 (12) (2007) 4338–4350.
[23] O. Théodoly, M. Jacquin, P. Muller, A.S. Chhun, Adsorption kinetics of amphiphilic diblock copolymers: from kinetically frozen colloids to macrosurfactants, Langmuir 25 (2) (2008) 781-793.
[24] S.C. Lee, H.J. Lee, pH-controlled, polymer-mediated assembly of polymer micelle nanoparticles, Langmuir 23 (2) (2007) 488–495.
[25] Y. Li, S. Zhang, H. Liu, Q. Li, W. Li, X. Huang, Synthesis and characterization of fluorine-containing PAA-b-PTPFCBPMA amphiphilic block copolymer, J. Polym. Sci. A 48 (23) (2010) 5419–5429.
[26] M. Burkhardt, N. Martinez-Castro, S. Tea, M. Drechsler, I. Babin, I. Grishagin, R. Schweins, D.V. Pergushov, M. Gradzielski, A.B. Zezin, Polyisobutylene-block-poly (methacrylic acid) diblock copolymers: self-assembly in aqueous media, Langmuir 23 (26) (2007) 12864–12874.
[27] I.-S. Choi, M. Park, E. Koo, S.-Y. Ju, Dispersions of carbon nanotubes by helical flavin surfactants: solvent induced stability and chirality enrichment, and solvatochromism, Carbon 184 (2021) 346–356.
[28] M. Bachilo Sergei, S. Strano Michael, C. Kittrell, H. Hauge Robert, E. Smalley Richard, R.B. Weisman, Structure-assigned optical spectra of single-walled carbon nanotubes, Science 298 (5602) (2002) 2361–2366.
[29] J. Polak, B.C.Y. Lu, Mutual solubilities of hydrocarbons and water at 0 and 25 °C, Can. J. Chem. 51 (24) (1973) 4018–4023.
[30] P. Nikolaev, M.J. Bronikowski, R.K. Bradley, F. Rohmund, D.T. Colbert, K.A. Smith, R.E. Smalley, Gas-phase catalytic growth of single-walled carbon nanotubes from carbon monoxide, Chem. Phys. Lett. 313 (1–2) (1999) 91–97.
[31] M.J. O'Connell, S.M. Bachilo, C.B. Huffman, V.C. Moore, M.S. Strano, E.H. Haroz, K.L. Rialon, P.J. Boul, W.H. Noon, C. Kittrell, J. Ma, R.H. Hauge, R.B. Weisman, R. E. Smalley, Band gap fluorescence from individual single-walled carbon nanotubes, Science 297 (5581) (2002) 593–596.
[32] A. Marini, A. Muñoz-Losa, A. Biancardi, B. Mennucci, What is solvatochromism?, J Phys. Chem. B 114 (51) (2010) 17128–17135.
[33] S. Nigam, S. Rutan, Principles and applications of solvatochromism, Appl. Spectrosc. 55 (11) (2001) 362A–370A.
[34] M.S. Strano, C.B. Huffman, V.C. Moore, M.J. O'Connell, E.H. Haroz, J. Hubbard, M. Miller, K. Rialon, C. Kittrell, S. Ramesh, R.H. Hauge, R.E. Smalley, Reversible, band-gap-selective protonation of single-walled carbon nanotubes in solution, J. Phys. Chem. B 107 (29) (2003) 6979–6985.
[35] G. Grundl, M. Müller, D. Touraud, W. Kunz, Salting-out and salting-in effects of organic compounds and applications of the salting-out effect of pentasodium phytate in different extraction processes, J. Mol. Liq. 236 (2017) 368–375.

**Supporting Information for**

# Larger Diameter Selection of Carbon Nanotubes by Two Phase Extraction using Amphiphilic Polymeric Surfactant

*Seokhyeon Son, Hyunjun Park, Woodong Jang*, Sang-Yong Ju**

Department of Chemistry, Yonsei University, 50 Yonsei-ro, Seodaemun-Gu, Seoul 03722, Korea

* Correspondence E-mail: wdjang@yonsei.ac.kr (W.-D.J.); syju@yonsei.ac.kr (S.-Y.J.)

**Figure S1**. $^{1}$H NMR spectrum of POBE-BzE.

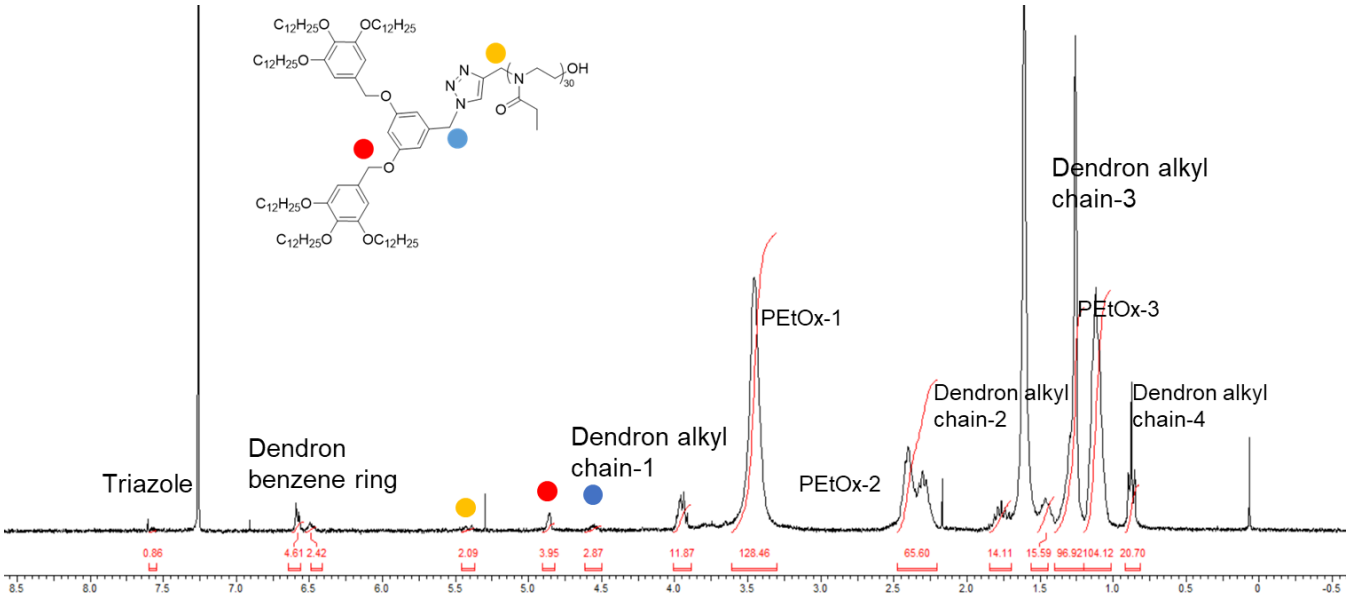


**Figure S2**. MALDI-TOF mass spectrum of POBE-BzE.

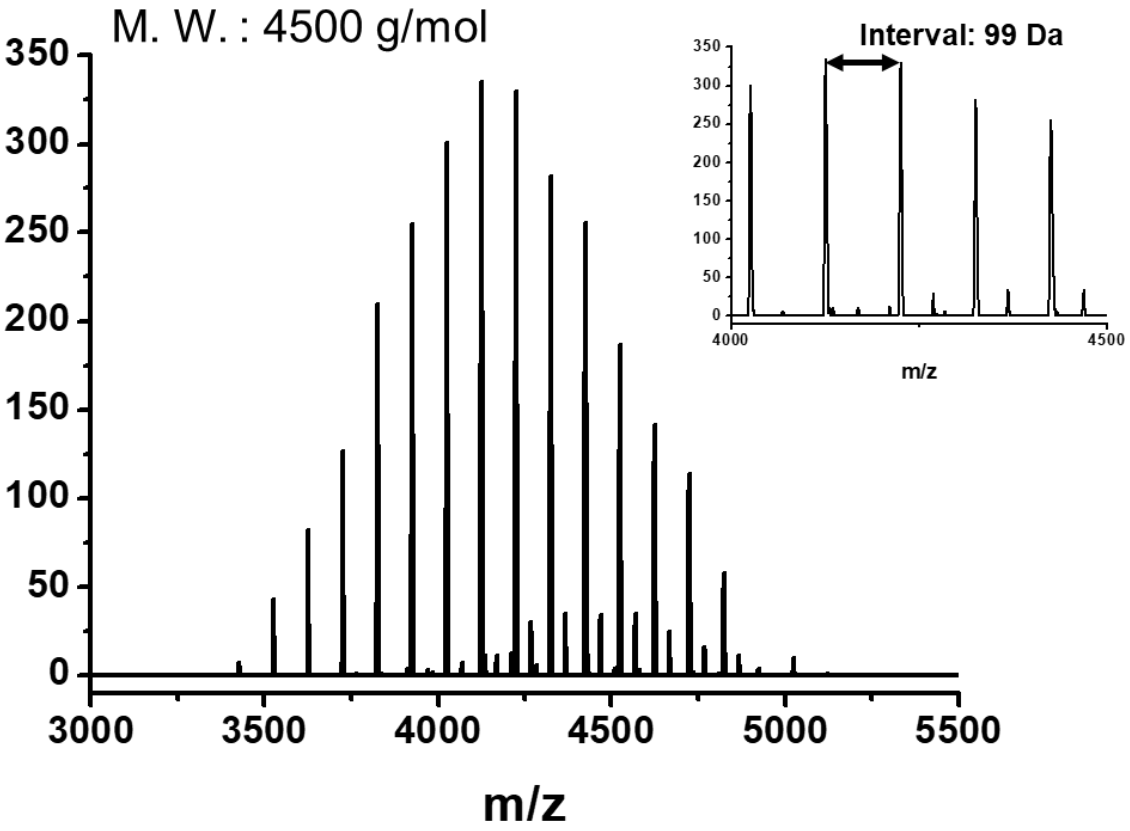

**Figure S3**. Elution profile of POBE-BzE by SEC.

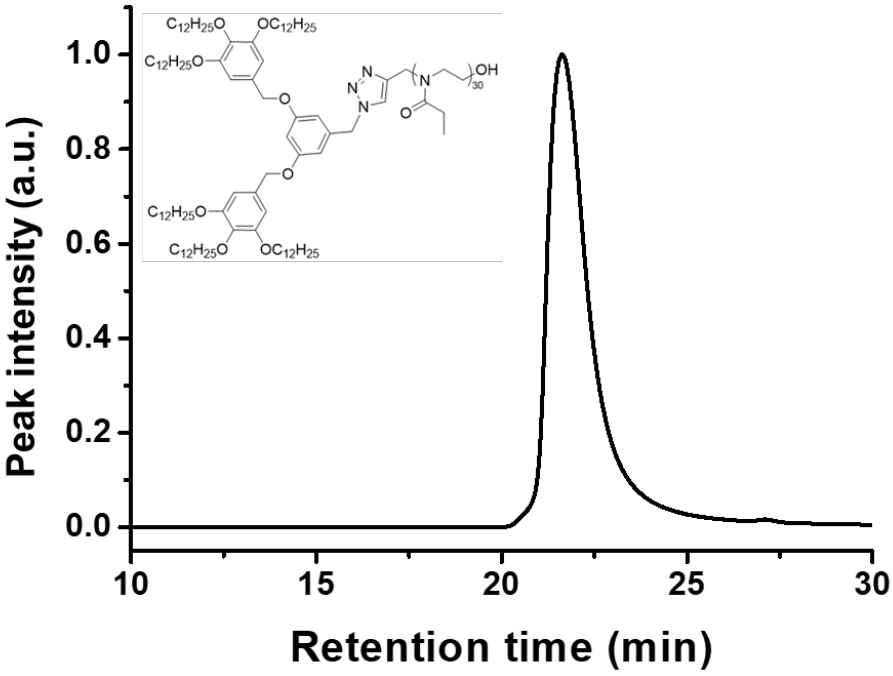


**Figure S4**. Solubility of various solvents in water [S1].

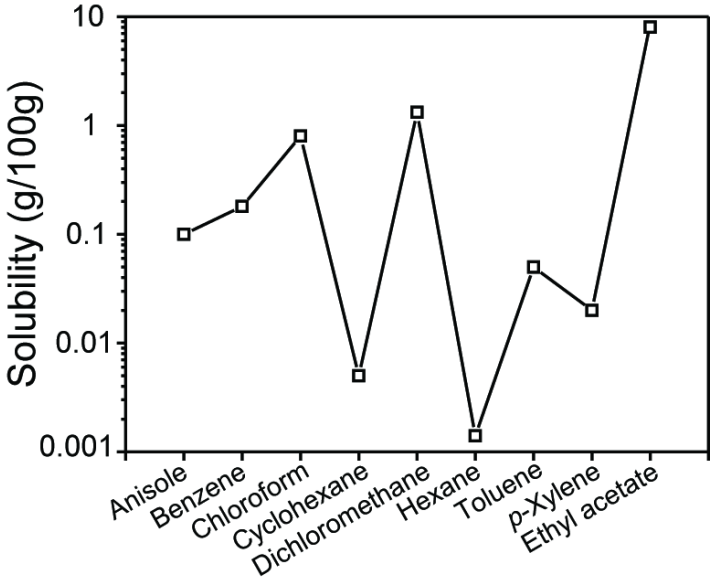

**Figure S5**. PL-based SWNT chirality abundances from (A) water and (B) *p*-xylene phases.

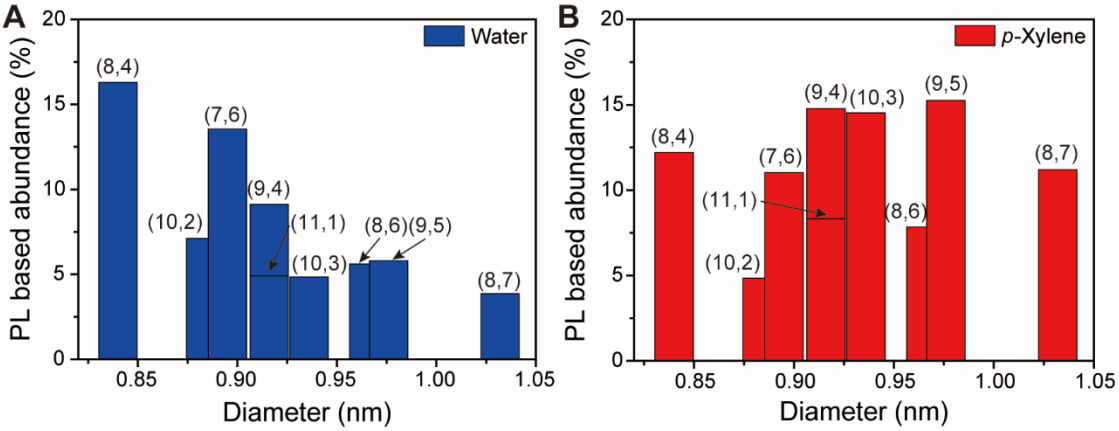


**Figure S6**. Attempt to disperse HiPco SWNT by using POBE. (A) Photograph of each layer. (B) Absorption spectra of water (black) and *p*-xylene (red) layers. The asterisks originate from residual water differences in blank and sample. (C) The corresponding PLE maps of each layers.

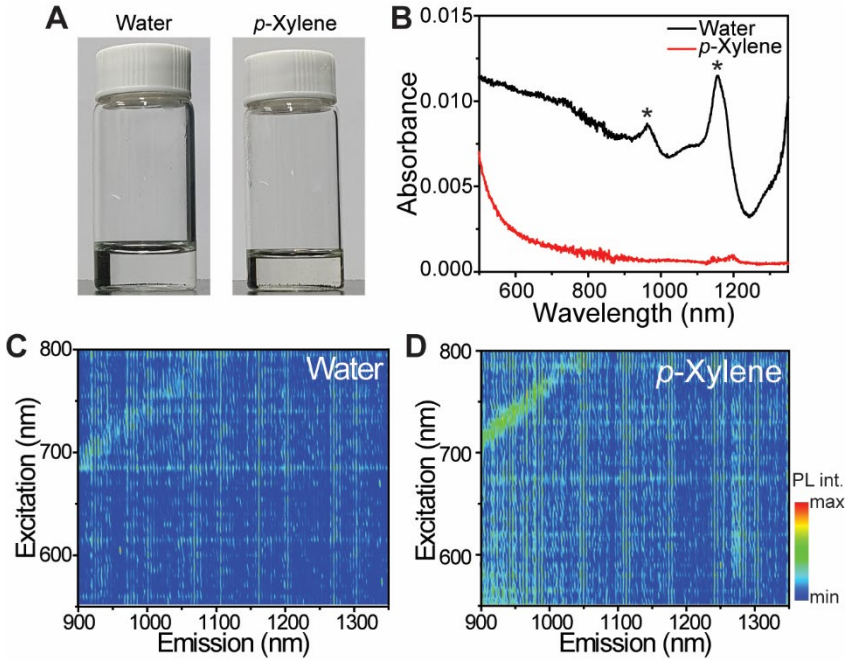

**Figure S7**. pH-dependent absorption and PL changes of POBE-BzE/SWNT/water dispersion. (A) Absorption spectra of POBE-BzE/HiPco in various pH. (B) The corresponding PLE maps.

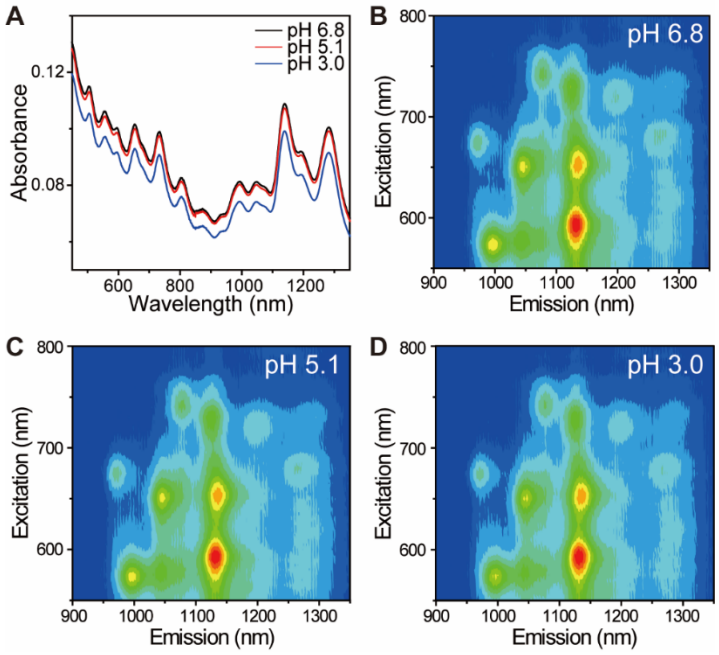

**Figure S8**. Offset absorption spectra of *p*-xylene after extraction with varying amounts of TBAB. Each spectrum is offset by 0.002 for visual clarity.

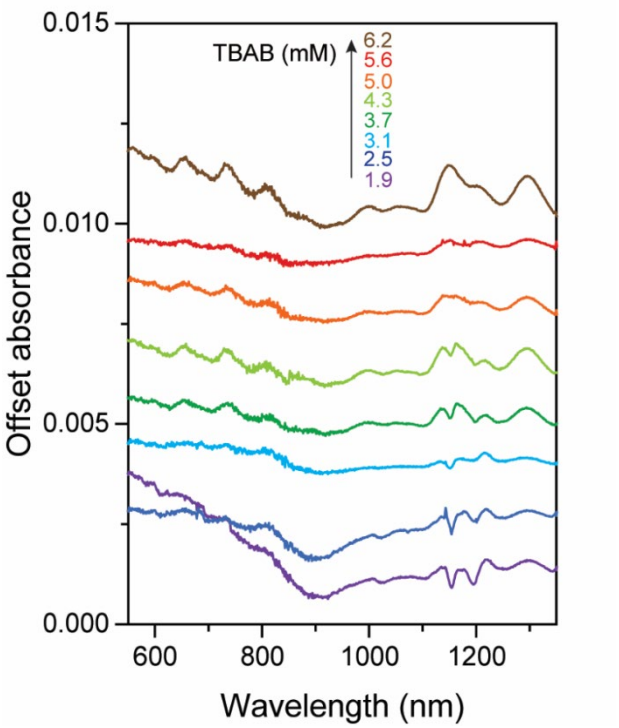


**Figure S9**. Determination of the peak (red line) from the background absorption.

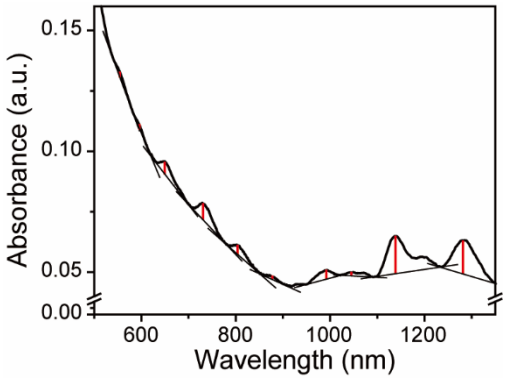

**Figure S10**. Preference of POBE-BzE in *p*-xylene against water. (A) POBE-BzE/SWNT/water dispersion (0.5 mL) and extraction with *p*-xylene (0.5 mL) containing 0, 7.4, 12.4, 17.4 and 22.4 mM. (B) Plot of POBE-BzE in *p*-xylene vs absorbance of POBE-BzE at 276 nm in water.

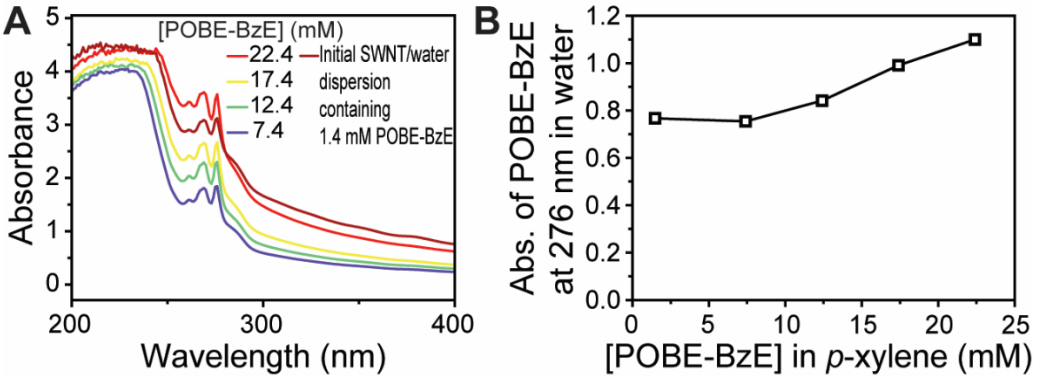

**Table S1**. Deconvoluted $e^{S}_{11}$ and $e^{S}_{22}$ of the SWNT chiralities in each dispersion.

| ($n$, $m$) | $d_t$ (nm) | Water dispersion | | *p*-Xylene dispersion | | Extracted water | | Extracted *p*-xylene | | $\Delta e^{S}_{11}$ between water/*p*-xylene (meV) | $\Delta e^{S}_{11}$ between extracted water/*p*-xylene (meV) |
|---|---|---|---|---|---|---|---|---|---|---|---|
| | | $e^{S}_{11}$ (nm) | $e^{S}_{22}$ (nm) | $e^{S}_{11}$ (nm) | $e^{S}_{22}$ (nm) | $e^{S}_{11}$ (nm) | $e^{S}_{22}$ (nm) | $e^{S}_{11}$ (nm) | $e^{S}_{22}$ (nm) | | |
| (6,5) | 0.76 | 995 | 573 | N/A | N/A | 994 | 574 | 995 | 568 | N/A | 1 |
| (8,3) | 0.78 | 972 | 674 | N/A | N/A | 971 | 672 | 964 | 674 | N/A | -9 |
| (7,5) | 0.83 | 1043 | 651 | N/A | N/A | 1045 | 650 | 1052 | 653 | N/A | 8 |
| (8,4) | 0.84 | 1131 | 592 | 1128 | 588 | 1132 | 593 | 1130 | 590 | -3 | -2 |
| (10,2) | 0.88 | 1075 | 743 | 1075 | 741 | 1074 | 740 | 1076 | 733 | 0 | 2 |
| (7,6) | 0.89 | 1135 | 654 | 1131 | 649 | 1137 | 652 | 1132 | 647 | -4 | -5 |
| (9,4) | 0.92 | 1125 | 727 | 1124 | 726 | 1124 | 730 | 1127 | 728 | -1 | 3 |
| (11,1) | 0.92 | 1287 | 618 | 1298 | 617 | 1285 | 619 | 1284 | 617 | 8 | -1 |
| (10,3) | 0.94 | 1274 | 634 | 1288 | 640 | 1278 | 641 | 1280 | 642 | 11 | 2 |
| (8,6) | 0.97 | 1200 | 722 | 1212 | 723 | 1198 | 723 | 1218 | 727 | 10 | 17 |
| (9,5) | 0.98 | 1266 | 680 | 1280 | 679 | 1269 | 680 | 1280 | 676 | 11 | 8 |
| (8,7) | 1.03 | 1288 | 733 | 1299 | 733 | 1291 | 735 | 1286 | 732 | 8 | -4 |
| Average $\Delta e^{S}_{11}$ | | | | | | | | | | 4 | 2 |

**Cited reference**

**S1.** S. J. Murov, Properties of Solvents Used in Organic Chemistry, accessed 11 May 2022,

<http://murov.info/orgsolvents.htm>